AMERICAN SOCIETY FOR MICROBIOLOGY | mBio®

RESEARCH ARTICLE

The PTS^{Ntr}-KdpDE-KdpFABC Pathway Contributes to Low Potassium Stress Adaptation and Competitive Nodulation of *Sinorhizobium fredii*

Xue-Ying Feng,[a,b] Yu Tian,[a,b] Wen-Jing Cui,[a,b] Yue-Zhen Li,[a,b] Dan Wang,[a,b] Yanbo Liu,[c] Jian Jiao,[a,b] Wen-Xin Chen,[a,b] Chang-Fu Tian[a,b]

[a]State Key Laboratory of Agrobiotechnology, and College of Biological Sciences, China Agricultural University, Beijing, China
[b]MOA Key Laboratory of Soil Microbiology, and Rhizobium Research Center, China Agricultural University, Beijing, China
[c]High School Affiliated to Renmin University, Beijing, China

ABSTRACT The rhizobium-legume symbiosis is essential for sustainable agriculture by reducing nitrogen fertilizer input, but its efficiency varies under fluctuating soil conditions and resources. The nitrogen-related phosphotransferase system (PTS^{Ntr}) consisting of PtsP, PtsO, and PtsN is required for optimal nodulation and nitrogen fixation efficiency of the broad-host-range *Sinorhizobium fredii* CCBAU45436 associated with diverse legumes, though the underlying mechanisms remain elusive. This work characterizes the PtsN-KdpDE-KdpFABC pathway that contributes to low potassium adaptation and competitive nodulation of CCBAU45436. Among three PtsN, PtsN$_1$ is the major functional homolog. The unphosphorylated PtsN$_1$ binds the sensory kinase KdpD through a non-canonical interaction with the GAF domain of KdpD, while the region covering HisKA-HATPase domains mediates the interaction of KdpD with the response regulator KdpE. KdpE directly activates the *kdpFABC* operon encoding the conserved high-affinity potassium uptake system. Disruption of this signaling pathway leads to reduced nodule number, nodule occupancy, and low potassium adaptation ability, but without notable effects on rhizoplane colonization. The induction of key nodulation genes *NIN* and *ENOD40* in host roots during early symbiotic interactions is impaired when inoculating the *kdpBC* mutant that shows delayed nodulation. The nodulation defect of the *kdpBC* mutant can be rescued by supplying replete potassium. Potassium is actively consumed by both prokaryotes and eukaryotes, and components of the PTS^{Ntr}-KdpDE-KdpFABC pathway are widely conserved in bacteria, highlighting the global importance of this pathway in bacteria-host interactions.

IMPORTANCE In all ecological niches, potassium is actively consumed by diverse prokaryotes and their interacting eukaryote hosts. It is only just emerging that potassium is a key player in host-pathogen interactions, and the role of potassium in mutualistic interactions remains largely unknown. This work is focused on the mutualistic symbiosis between rhizobia and legumes. We report that the nitrogen-related phosphotransferase system PTS^{Ntr}, the two-component system KdpDE, and the high-affinity potassium uptake system KdpFABC constitute a pathway that is important for low potassium adaptation and optimal nodulation of rhizobia. Given the widely conserved PTS^{Ntr}, KdpDE, and KdpFABC in bacteria and increasing knowledge on microbiome for various niches, the PTS^{Ntr}-KdpDE-KdpFABC pathway can be globally important in the biosphere.

KEYWORDS legume, potassium, soybean, symbiosis

Protein phosphorylation is one of the major mechanisms underlying organisms' adaptation to fluctuating conditions and resources in various ecological niches. Bacterial kinases can be classified into four major families (1). The eukaryote-like protein kinases (also referred to

Invited Editor Anke Becker, Philipps University Marburg

Editor Joerg Vogel, University of Würzburg

Address correspondence to Chang-Fu Tian, cftian@cau.edu.cn.

The authors declare no conflict of interest.

Received 11 March 2022
Accepted 13 April 2022
Published 2 May 2022

Hanks-type kinases) phosphorylate a large spectrum of substrates at their serine and threonine residues (2). The BY kinases catalyze phosphorylation of targets at tyrosine residues (3). The two-component systems include a sensory histidine kinase that autophosphorylates at a conserved histidine by using the γ-phosphoryl group of ATP, and a response regulator that receives the phosphoryl from the histidine-phosphorylated kinase at a conserved aspartate residue (4). The fourth family is the phosphotransferase system harboring a group of enzymes that sequentially transfer the phosphoryl group derived from phosphoenolpyruvate to a histidine residue of downstream members of the system (5). The canonical phosphotransferase system (PTS) directly involved in carbohydrate uptake (6, 7) and the nitrogen-related phosphotransferase system (PTS^{Ntr}) have been found in various bacteria. Both canonical PTS and PTS^{Ntr} have enzyme I (EI or EI^{Ntr}), histidine protein (HPr or NPr), and enzyme II (EIIA or $EIIA^{Ntr}$), while the PTS^{Ntr} lacks substrate specific EIIB and EIIC required for carbohydrate uptake (5). The PTS^{Ntr} is characterized by its regulatory roles in diverse processes such as the metabolism of nitrogen and carbon, phosphate starvation, and K^+ homeostasis (5, 8, 9).

K^+ selective cation channels are essential for both prokaryotes and eukaryotes to maintain the asymmetric K^+/Na^+ distribution, with K^+ as the major cation in the cytoplasm while Na^+ being dominant in the media (10). Bacteria usually harbor a variable number of K^+ uptake systems including Trk, Ktr, Kup, and Kdp reflecting adaptations to different niches (11, 12). The H^+-dependent Trk and Na^+-dependent Ktr show low cation selectivity with moderate binding affinity, while the K^+ uptake permease Kup and the P-type ATPase mediating system Kdp are considered specific K^+ transporters with Kdp being the high-affinity K^+ transporter (11, 12). Moreover, *kdp* genes are inducible under low K^+ conditions where the sensor kinase KdpD phosphorylates the response regulator KdpE that promotes transcription of the *kdpFABC* operon (13, 14). Although the precise signal recognized by the membrane-bound KdpD is still under discussion (14), it has been demonstrated that unphosphorylated $EIIA^{Ntr}$ can interact with KdpD in *Escherichia coli*, *Rhizobium leguminosarum*, and *Pseudomonas putida* and activates the transcription of *kdpFABC* genes (15–17). With evidences from mutants of K^+ uptake systems of *Salmonella* (18), *Staphylococcus aureus* (19), *Helicobacter pylori* (20), *Mycobacterium tuberculosis* (21), *Pectobacterium wasabiae* (22), *Streptococcus mutans* (23), and *Sinorhizobium meliloti* (24), it is only just emerging that K^+ is an environmental cue and a key player in host-bacteria interactions (25, 26).

These studies imply that a PTS^{Ntr}-KdpDE-KdpFABC pathway might be involved in host-bacteria interactions, though not fully established in any individual system yet. To test this hypothesis, we focused on the mutualistic interactions between rhizobia and legumes which innovate root nodules where rhizobia reduce atmospheric nitrogen into ammonia to support plant growth (27, 28). Our previous work reveals that PTS^{Ntr} is essential for effective symbiosis of *Sinorhizobium fredii* CCBAU45436 with soybean and pigeon pea plants (29). The symbiotic defects of mutants lacking EI^{Ntr} (*ptsP*) or Npr (*ptsO*) can be partially rescued by further deletion of an $EIIA^{Ntr}$ ($ptsN_1$) while the single $ptsN_1$ mutant is indistinguishable from the wild-type strain except impaired nodulation and nodule occupancy abilities (29). In this work, we aimed to characterize the $EIIA^{Ntr}$-KdpDE-KdpFABC pathway in CCBAU45436, and investigate the potential role of Kdp in symbiotic interactions. Three PtsN homologs were characterized for their effect on symbiosis and low potassium adaptation, and ability to interact with KdpD. Distinct domains of KdpD involved in interactions with the major $EIIA^{Ntr}$ ($PtsN_1$) and KdpE were identified, and direct activation of the *kdpFABC* operon by KdpE was demonstrated. The effects of phosphorylated or unphosphorylated $PtsN_1$ and the downstream KdpDE-KdpFABC pathway in low potassium adaptation and symbiotic interactions were further characterized. Together with the transcriptional analysis of key nodulation genes of soybean plants during early interaction stages and nodulation kinetics assay, the important role of K^+ uptake in optimal nodulation mediated by the PTS^{Ntr}-KdpDE-KdpFABC pathway is proposed and discussed.

RESULTS AND DISCUSSION

Expansion of PtsN homologs in *Rhizobiaceae*. The regulatory roles of PTS^{Ntr} have been intensively studied in various pathogens, with PtsN being the major output regulator

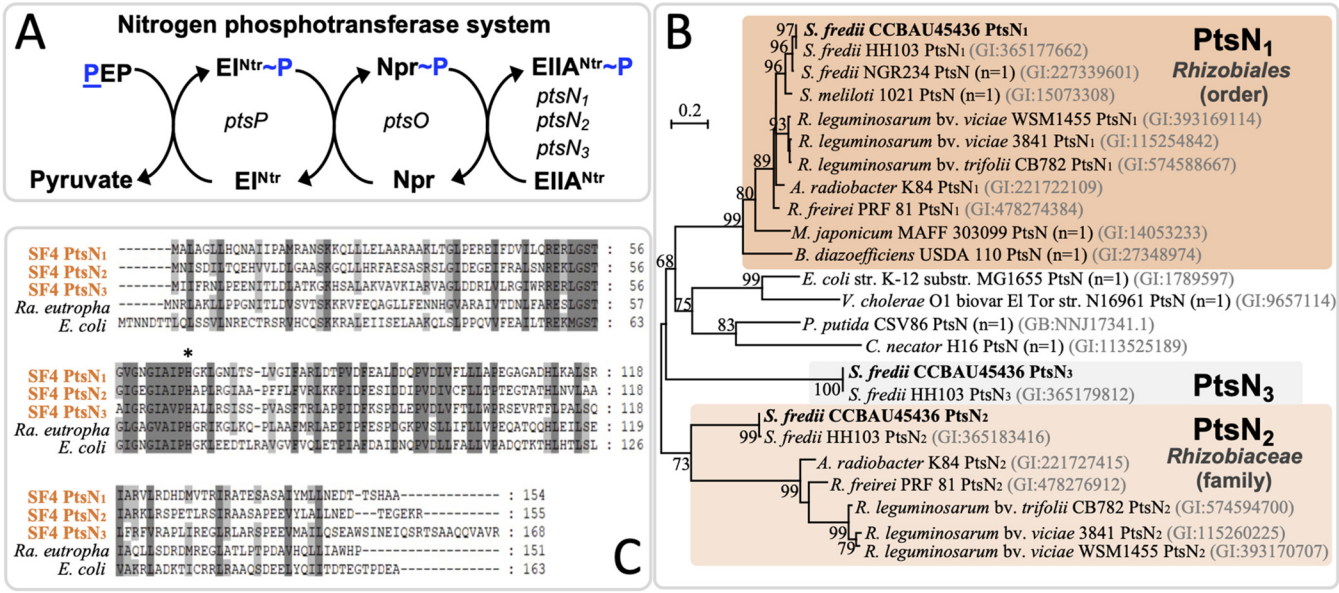

FIG 1 PtsN homologs in *Sinorhizobium fredii* CCBAU45436. (A) Components of PTS^{Ntr} in *S. fredii* CCBAU45436 (SF4) including *ptsP* encoding EI^{Ntr}, *ptsO* encoding Npr, and three copies of *ptsN* encoding $EIIA^{Ntr}$. (B) The unrooted maximum likelihood phylogenetic tree of $EIIA^{Ntr}$ homologs from representative bacterial species. Bootstrap values above 60 are shown. *n* = 1 indicates that only one $EIIA^{Ntr}$ can be identified in the corresponding strain. *R*, *Rhizobium*; *S*, *Sinorhizobium*; *A*, *Agrobacterium*; *M*, *Mesorhizobium*; *B*, *Bradyrhizobium*; *E*, *Escherichia*; *V*, *Vibrio*; *P*, *Pseudomonas*; *C*, *Cupriavidus*. (C) Alignment of PtsN homologs showing the conserved histidine (*, H66 in SF4 $EIIA^{Ntr}$) involved in phosphorylation (~P). PtsN homologs of *Ralstonia eutropha* H16 and *E. coli* MG1655 are included for comparison.

(5). The broad-host-range rhizobium *S. fredii* CCBAU45436 (SF4 hereafter) (30–32) has three PtsN homologs (Fig. 1A). Phylogenetic analysis indicated their distinct phyletic distribution (Fig. 1B), with $PtsN_1$ conserved in the *Rhizobiales* order (including genera *Rhizobium*, *Sinorhizobium*, *Agrobacterium*, *Mesorhizobium*, and *Bradyrhizobium*) and clustered with PtsN from other bacteria in a highly supported orthologous group, with $PtsN_2$ present in some species of the *Rhizobiaceae* family, and with $PtsN_3$ identified in *S. fredii* strains SF4 and HH103. Although $PtsN_1$, $PtsN_2$, and $PtsN_3$ of SF4 belong to three separate clusters (Fig. 1B), sequence alignment analysis (Fig. 1C) showed that they have the conserved histidine residue (H66) which is the only phosphorylated site of $EIIA^{Ntr}$ homologs as demonstrated previously (33). To investigate the potential role of the three *ptsN* homologs of SF4 in symbiosis, all single, double and triple in-frame deletion mutants were constructed and tested for their symbiotic performance on soybean plants (Table S1). All test mutants were able to form functional nodules which supported the growth of soybean plants at a similar level as the wild-type SF4 regarding shoot dry weight and leaf chlorophyll content (Table S1; ANOVA followed by Duncan's test, alpha = 0.05). The $ptsN_1$, $ptsN_{12}$, $ptsN_{13}$, $ptsN_{123}$, and $ptsN_2$ mutants formed similar numbers of nodules which were significantly less than those induced by SF4, $ptsN_3$, and $ptsN_{23}$ mutants (ANOVA followed by Duncan's test, alpha = 0.05). This suggests that PtsN homologs are important for optimal nodulation of *S. fredii* on soybean plants, with the more conserved $PtsN_1$ being the major functional homolog and the positive effect of $PtsN_2$ depending on the presence of $PtsN_3$. This is in line with the finding in *R. leguminosarum* which harbors two PtsN homologs with $PtsN_1$ as the major $EIIA^{Ntr}$ (9).

Notably, a *R. leguminosarum* mutant lacking functional $EIIA^{Ntr}$ formed a similar number of nodules as the wild-type strain but fixed less nitrogen on pea plants while *S. fredii* lacking $EIIA^{Ntr}$ formed fewer effective nodules on soybean plants (Table S1) (9, 29). This contrasting phenotype may be at least partially due to different stimuli encountered by rhizobia during the establishment and maintenance of the determinate (with transient meristems, such as soybean and cowpea) and indeterminate nodules (with persistent meristems, such as pea and alfalfa) (34, 35). Rhizobia terminally differentiate (enlarged cell size and reduced reproductive ability) in pea and alfalfa nodules but not in soybean and cowpea nodule cells (27, 36–38). Nitrogen-fixing rhizobial cells accumulate more carbon storage polymer

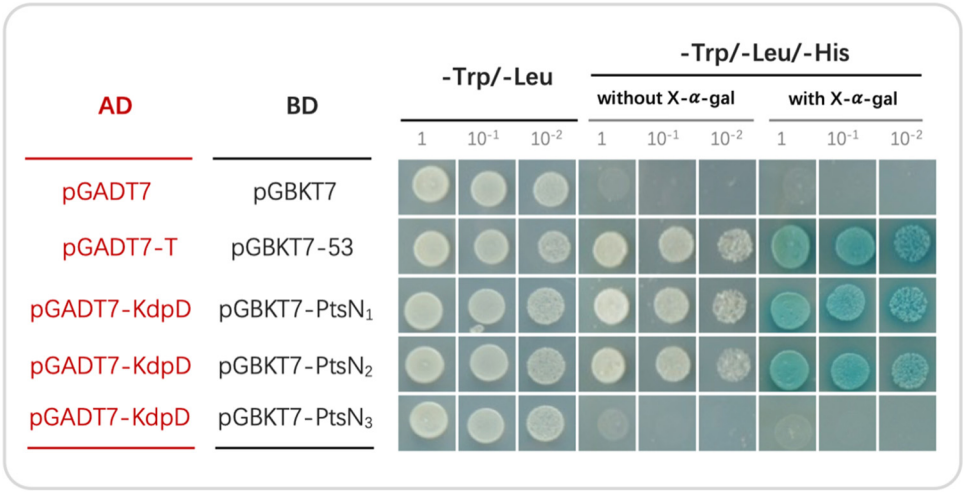

FIG 2 $PtsN_1$ and $PtsN_2$ directly interact with KdpD. Three dilutions are shown from the yeast two-hybrid experiment with pGADT7/pGBKT7 and pGADT7-T/pGBKT7-53 as negative and positive controls, respectively. Yeast cells were co-transformed with AD and BD vectors. The growth on the medium lacking Trp/Leu/His, and blue color indicate protein interaction.

poly-β-hydroxybutyrate (PHB) in soybean and cowpea nodules than in pea and alfalfa nodules (27, 36–38). We have revealed that PHB biosynthesis and nitrogen fixation is blocked in the *ptsP* and *ptsO* mutants but restored in the $ptsPN_1$ and $ptsON_1$ double mutants of *S. fredii* in soybean nodules (29). Although the regulation of nitrogen and carbon metabolism by PTS^{Ntr} is supported by evidences from both *S. fredii*-soybean and *R. leguminosarum*-pea symbioses (9, 29), the underlying signaling pathway mediated by PTS^{Ntr} in PHB biosynthesis and other adaptive processes in these contrasting rhizobium-legume pairs remains elusive.

$PtsN_1$ and $PtsN_2$ interact with KdpD and contribute to low potassium adaptation and optimal nodulation. As the interaction between $EIIA^{Ntr}$ and KdpD has been recurrently found in *E. coli*, *R. leguminosarum*, and *Pseudomonas putida* (15–17), the yeast two-hybrid experiment was used herein to identify which PtsN homolog(s) may keep this conserved function. It turned out that $PtsN_1$ and $PtsN_2$ rather than $PtsN_3$ interact with KdpD under test conditions (Fig. 2). After an exploring test of different levels of K^+ (Fig. S1), 1 μM and 10 mM was considered as low and replete K^+ conditions, respectively. Under the low K^+ condition (1 μM K^+), the $ptsN_{12}$ mutant exhibited a more severe growth defect than the $ptsN_1$ or $ptsN_2$ mutants (Fig. 3A), implying cumulative effects associated with $PtsN_1$ and $PtsN_2$. Similarly, the $ptsN_{123}$ mutant grew worse than the $ptsN_{13}$ mutant that in turn grew worse than the $ptsN_3$ mutant. Noteworthy, growth delay was observed for the $ptsN_1$ mutant but not for the $ptsN_2$, $ptsN_3$, and $ptsN_{23}$ mutants, suggesting $PtsN_1$ as the major $EIIA^{Ntr}$. Although the $ptsN_3$ mutant was indistinguishable from SF4, the $ptsN_{123}$ and $ptsN_{13}$ mutants grew slightly better than the $ptsN_{12}$ and $ptsN_1$ mutants, respectively, indicating a potential negative regulatory role of $PtsN_3$ in low K^+ adaptation. On the other hand, the growth rate of all test strains was higher under K^+ replete condition (10 mM K^+) than low K^+ condition (Fig. 3A). $PtsN_1$ was required for the maximum growth rate of SF4 under this K^+ replete condition likely due to its regulatory roles in carbon metabolism (16, 29), with cumulative contribution by $PtsN_2$ and antagonistic effect from $PtsN_3$. The strong synthetic negative phenotype of the $ptsN_{12}$ mutant under low K^+ condition was however not observed under this K^+ replete condition. Moreover, the *ptsP* and *ptsO* mutants grew faster than the $ptsN_{12}$ and $ptsN_{123}$ mutants under low K^+ condition while the reverse was observed under K^+ replete condition (Fig. 3A), suggesting a regulatory duality mediated by switching $EIIA^{Ntr}$ phosphorylation status (Fig. 1A) (5). These results, particularly the contrasting growth phenotypes of the $ptsN_{12}$ mutant under K^+ replete and deplete conditions, implied that $EIIA^{Ntr}$ is critical for *S. fredii* adaptation to fluctuating levels of K^+ that is also consumed by other organisms in the same habitat including the interacting eukaryote hosts (25, 26, 39).

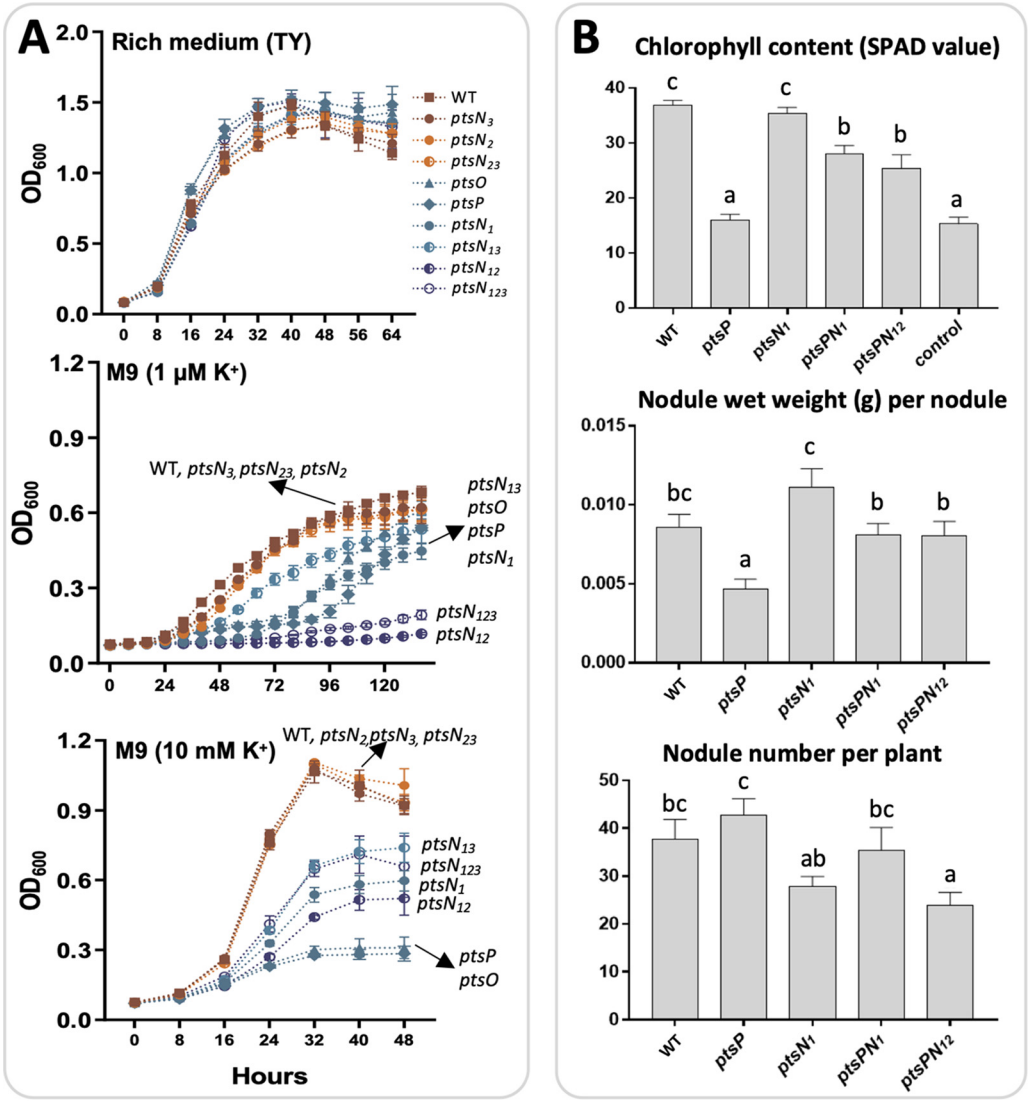

FIG 3 Cumulative role of $ptsN_1$ and $ptsN_2$ in low K^+ adaptation and nodulation. (A) Growth curves in rich medium and minimum medium supplied with 1 μM and 10 mM K^+. Results are based on average ± SEM of three biological replicates. (B) Symbiotic performance on soybean plants. Different letters indicate significant difference between treatments (Average ± SEM; ANOVA followed by Duncan's test, alpha = 0.05). More than eight plants were scored.

The *ptsP* mutant has pleiotropic defects including symbiotic inefficiency which can be partially rescued by further deletion of $ptsN_1$ (29). To investigate whether the second KdpD-interacting $EIIA^{Ntr}$ $PtsN_2$ has cumulative contribution to symbiotic efficiency, the triple mutant $ptsPN_{12}$ was constructed. This mutant was as efficient as the $ptsPN_1$ mutant and performed better than the *ptsP* mutant regarding chlorophyll content of inoculated soybean plants (ANOVA followed by Duncan's test, alpha = 0.05), though shoot dry weight was partially recovered in the $ptsPN_1$ and $ptsPN_{12}$ treatments at an insignificant level under test conditions (Fig. 3B; Table S2). Inefficient nodules induced by the *ptsP* mutant were significantly smaller than those efficient nodules formed by SF4, $ptsN_1$, $ptsPN_1$ and $ptsPN_{12}$ mutants (Fig. 3B; Table S2). The $ptsN_1$ and $ptsPN_{12}$ mutants formed significantly less nodules than the *ptsP* and $ptsPN_1$ mutants, respectively. It seems that the contrasting number and weight of nodules between the *ptsP* and $ptsN_1$ treatments are in line with the canonical model of autoregulation of nodulation (28). However, nodule weight was similar between the $ptsPN_1$ and $ptsPN_{12}$ treatments (Fig. 3B; Table S2), indicating that the reduced nodule number in the $ptsPN_{12}$ treatment compared with the $ptsPN_1$ treatment may also be regulated by processes other than autoregulation of nodulation. Therefore, a cumulative role of $PtsN_2$ in optimal

nodulation was revealed by comparing the *ptsP*, *ptsPN$_1$*, and *ptsPN$_{12}$* mutants. Taken together with the nodulation phenotypes and growth curves of various *ptsN* mutants (Table S1; Fig. 3), despite an expansion of PtsN copies in the *Rhizobiaceae* family (Fig. 1B), these findings suggest $PtsN_1$ as the major $EIIA^{Ntr}$ in symbiotic interaction and low K^+ adaptation with a cumulative contribution by $PtsN_2$.

Optimal nodulation and low potassium adaptation mediated by the $EIIA^{Ntr}$-Kdp pathway. All known regulatory roles of $EIIA^{Ntr}$ are mediated by its phosphorylation status of H66 (Fig. 1C) (8, 33, 40–42). Here we constructed the *ptsN$_1$(H66A)* and *ptsN$_1$(H66E)* strains harboring non-phosphorylated $PtsN_1$ and phosphorylated $PtsN_1$, respectively. Similar to the *ptsN$_1$* mutant, the *ptsN$_1$(H66E)* strain formed less nodules than the wild-type SF4, the *ptsP* mutant, and the *ptsN$_1$(H66A)* strain while showing no significant difference in symbiotic performance regarding leaf chlorophyl content and shoot dry weight compared with these strains except the inefficient *ptsP* mutant (Fig. 4A; Table S3). Moreover, the *ptsN1(H66A)* strain and the *ptsP* mutant induced smaller nodules than the *ptsN$_1$(H66E)* strain, the *ptsN$_1$* mutant, and SF4 (Fig. 4A; Table S3). Therefore, the involvement of $PtsN_1$ in optimal nodulation is mediated by the phosphorylation status of its H66 residue.

Because the major $EIIA^{Ntr}$ $PtsN_1$ directly interacts with KdpD (Fig. 2), we wonder if the KdpDE-KdpFABC pathway is involved in optimal nodulation mediated by phosphorylation status of $PtsN_1$. Yeast two-hybrid experiment showed that $PtsN_1$(H66E) failed to interact with KdpD while $PtsN_1$(H66A) can interact with KdpD though at a relatively lower efficiency compared with the wild-type $PtsN_1$ (Fig. 4B). The interaction between unphosphorylated $EIIA^{Ntr}$ and KdpD is consistent with the findings in other bacteria including *E. coli* and *R. leguminosarum* (15, 16).

The *kdpDE* and *kdpFABC* operons have a widely conserved synteny in various bacteria (43). In SF4 genome, the *kdpD* gene has four overlapping nucleotides with the downstream coding region of the response regulator KdpE (Fig. 4C), and reverse transcription-PCR analysis revealed that *kdpF*, *kdpA*, *kdpB*, and *kdpC*, encoding the high-affinity K^+ uptake system, constitute an operon (Fig. 4C). To test the potential role of KdpDE and KdpFABC in nodulation, *kdpDE* and *kdpBC* were deleted in backgrounds of WT, *ptsP*, or *ptsO* mutants. All mutants lacking *kdpBC* formed less nodules compared with their parent strains whereas the decrease of nodule number for mutants lacking *kdpDE* was not statistically significant (Fig. 4D; Table S4), suggesting the requirement of high-affinity K^+ uptake in optimal nodulation and potential complementary effects by other K^+ uptake systems in the *kdpDE* mutant (see below for transcriptional profiles of different K^+ uptake systems). The *kdp* mutants had similar symbiotic performance as their parent strains regarding leaf chlorophyll content and shoot dry weight (Table S4). When replete K^+ (10 mM) was supplied in the rhizosphere, nodulation defects of the *kdpBC* and *ptsN$_1$(H66E)* strains can be largely rescued (Fig. 4E). These results suggest that $EIIA^{Ntr}$ and its downstream high-affinity K^+ uptake system are involved in optimal nodulation on soybean plants. The involvement of K^+ uptake system in modulating nodulation is also observed for *S. meliloti* associated with alfalfa (24) where the double mutant of low affinity K^+ uptake systems Trk and Kup (14) exhibited delayed nodulation that was further enhanced in the *trk-kup-kdp* triple mutant. In line with the findings in this work on *S. fredii*-soybean system, these *S. meliloti* mutants of K^+ uptake systems formed nitrogen fixing nodules on alfalfa (24), supporting the role of K^+ uptake during early symbiotic interactions.

In the *S. meliloti*-alfalfa system, it has been shown that the low affinity Trk and Kup systems are required for competitive nodulation (24). In this work, nodule occupancy assay on soybean plants (Fig. 5A) revealed that *S. fredii* mutants lacking *kdpBC* or *kdpDE* were outcompeted by their corresponding parent strains (WT, the *ptsP*, or *ptsO* mutants) while the *ptsN$_1$(H66A)* strain rather than *ptsN$_1$(H66E)* was as competitive as the wild-type SF4. Further analysis of survival rate (CFU) on rhizoplane showed that the observed contrasting competitive nodulation abilities among test strains (Fig. 4A; Fig. 4D; Fig. 5A) cannot be fully explained by their rhizoplane colonization rates (Fig. 5A). For example, rhizoplane CFU of the *kdpDE*, *ptsO-kdpDE*, and *ptsO-kdpBC* mutants were comparable with those of the corresponding parent strains. These findings imply a more active role of $EIIA^{Ntr}$-Kdp pathway during symbiotic interactions than in root colonization.

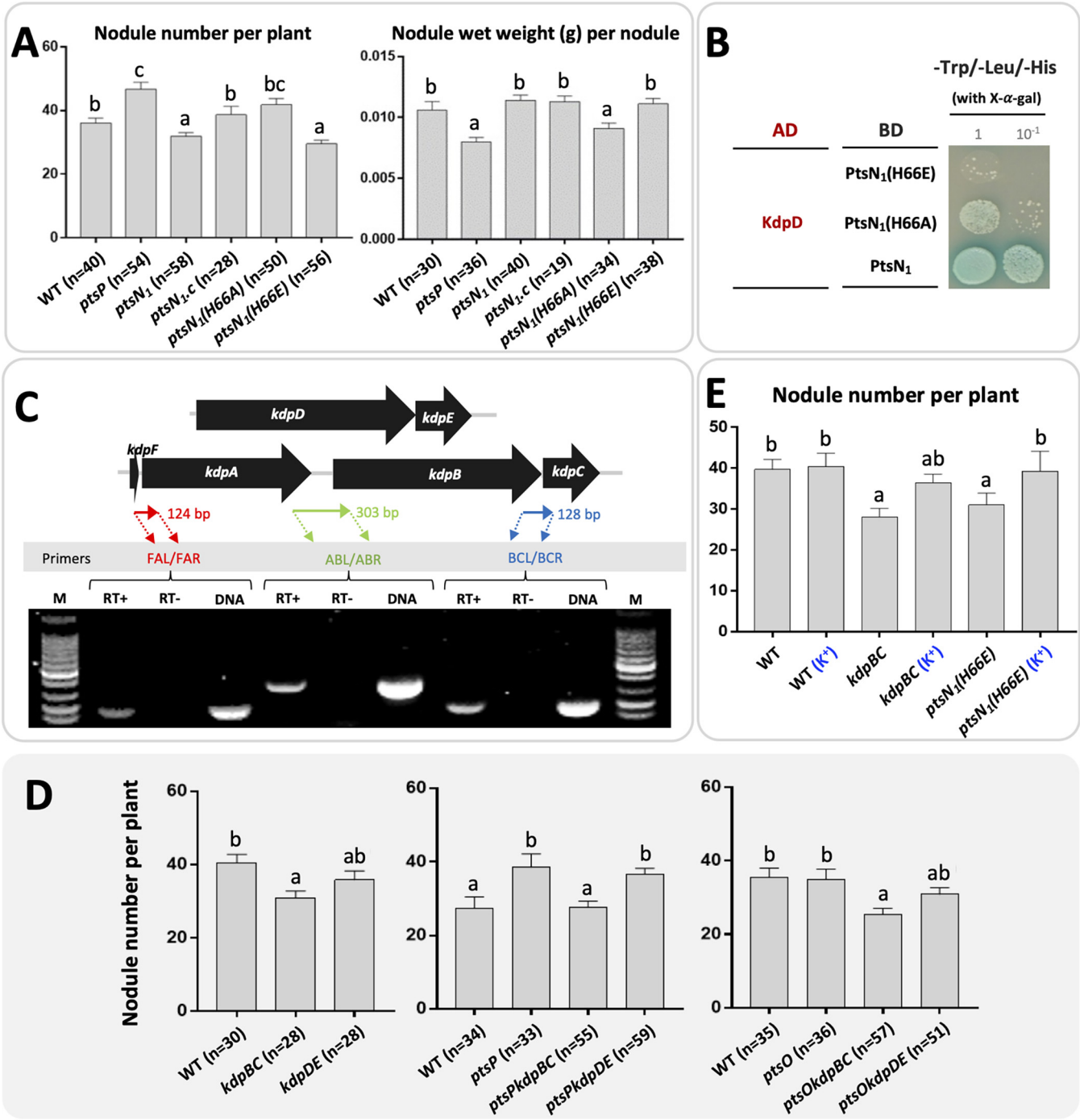

FIG 4 PTS^{Ntr} and KdpBC are required for optimal nodulation. (A) Nodulation characteristics of strains carrying *ptsN$_1$(H66A)* or *ptsN$_1$(H66E)*. The number of scored plants from multiple independent experiments is shown in brackets. (B) PtsN$_1$(H66A) directly interacts with KdpD. Two dilutions are shown from the yeast two-hybrid experiment with the negative (pGADT7 and pGBKT7) and positive (pGADT7-T and pGBKT7-53) controls as shown in Fig. 2 (C) Cotranscription of the *kdpFABC* operon of SF4 grown in minimum medium (M9). The fragments covering corresponding intergenic regions targeted by three pairs of primers are indicated and amplified in RT-PCR. Reverse transcriptase was added to the reaction in RT+, but omitted from reactions in RT-. Genomic DNA was amplified as a positive control. M, 100 bp marker. (D) Deletion of *kdpBC* rather than *kdpDE* in the wild-type SF4 (WT), the *ptsP* or *ptsO* mutants leads to less nodules formed on soybean plants. The number of scored plants is indicated in brackets. (E) Nodulation defects of the *kdpBC* mutant and the *ptsN$_1$(H66E)* strain can be rescued by supplying replete K$^+$ (10 mM) in the rhizosphere (more than 10 plants were scored). (A) and (D to E), different letters indicate significant difference between treatments (Average ± SEM; ANOVA followed by Duncan's test, alpha = 0.05).

To verify if the test mutants with nodulation defects are also impaired in low K$^+$ adaptation, their growth curves were compared (Fig. 5B). Consistent with the predicted role of KdpDE and KdpFABC in low K$^+$ adaptation ($< 100\ \mu$M) (14, 44), the *kdpDE* and *kdpBC* mutants were unable to grow in the minimum medium containing 1 μM K$^+$ while

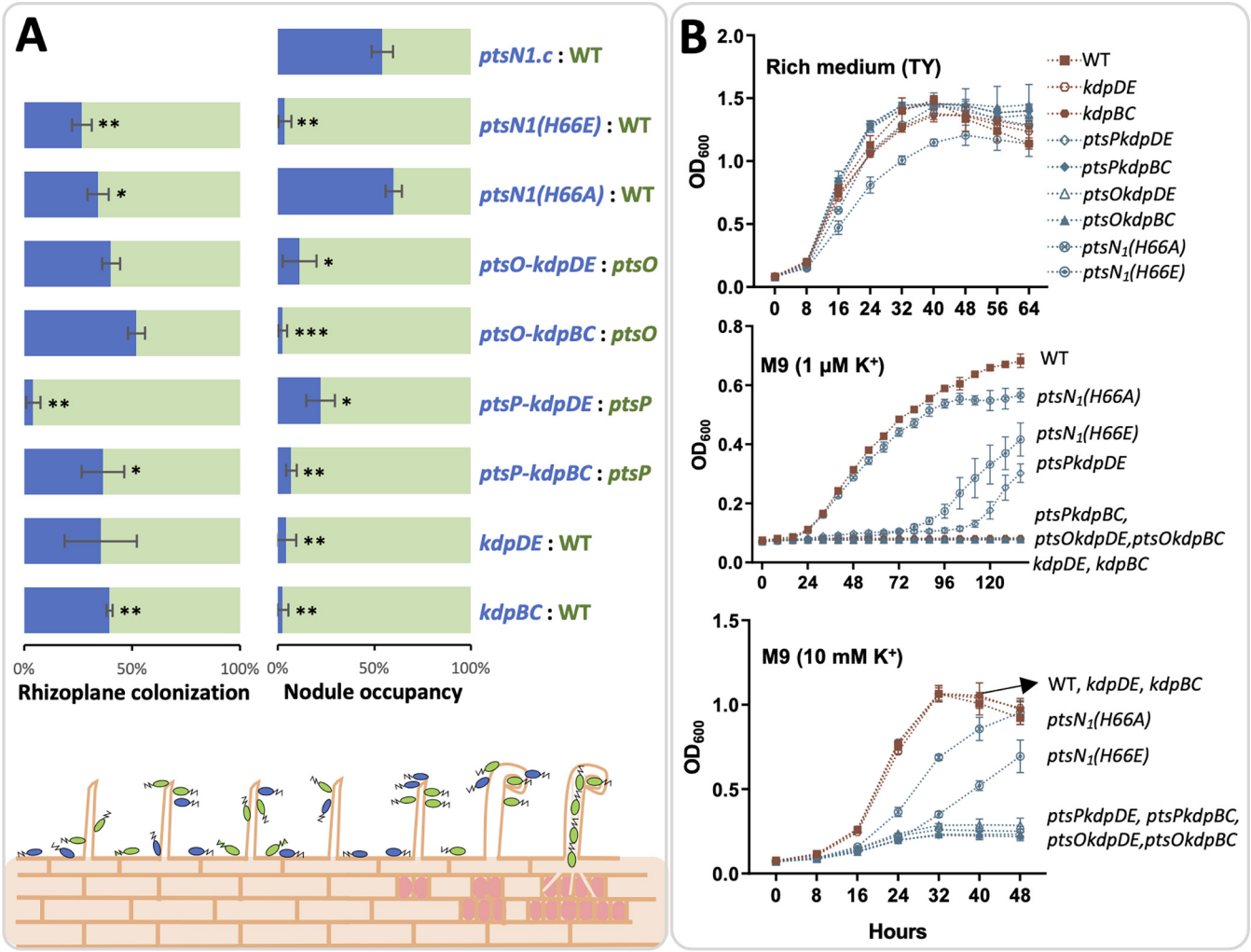

FIG 5 PTS^{Ntr} and Kdp system are required for nodule occupancy and low potassium adaptation. (A) Rhizoplane colonization and nodule occupancy by pairs of mixed inoculants (1:1 ratio within each pair). Significant difference is indicated based on one sample *t* test (theoretical mean = 0.5; *, $P < 0.05$; **, $P < 0.01$; ***, $P < 0.001$). Error bars represent SD of three biological replicates. (B) The growth curves of various derivatives of *S. fredii* CCBAU45436 (SF4) in the TY rich medium, M9 minimum medium with 1 μM or 10 mM K$^+$.

indistinguishable from the wild-type SF4 when replete K$^+$ (10 mM) was supplied (Fig. 5B). Similarly, the *ptsP* or *ptsO* derivatives lacking either *kdpBC* or *kdpDE* showed significant growth defects under the low K$^+$ condition (Fig. 5B), which can be rescued to the level of the *ptsP* and *ptsO* mutants (Fig. 3A) by supplying replete K$^+$ (Fig. 5B). Under the low K$^+$ condition, the *ptsN$_1$(H66A)* strain grew at a similar rate as SF4 before reaching stationary phase while the *ptsN$_1$(H66E)* strain showed a significant growth delay (Fig. 5B) that can be rescued to the level of the *ptsN$_1$* mutant (Fig. 3A) by adding 10 mM K$^+$ (Fig. 5B). It is also noteworthy that the unphosphorylated PtsN$_1$ allowed better growth than the *ptsP* and *ptsO* mutants under the low K$^+$ condition (Fig. 4B and Fig. 3A). This can be partially explained by EIIA^{Ntr}-independent output signals derived from EI^{Ntr} and Npr as indicated in the carbon source utilization characteristics of related mutants of SF4 (29) and potential cross talk between the canonical PTS and PTS^{Ntr} in modulating the KdpDE-KdpFABC pathway as shown in *E. coli* (15, 45). Despite the complexity in the upstream signaling components, the unphosphorylated form of PtsN$_1$ is notably essential for low K$^+$ adaptation through interacting with KdpD (Fig. 5B and Fig. 4B).

KdpD interacts with KdpE and PtsN$_1$ in a non-canonical way. The interaction between KdpD and PtsN$_1$ has been demonstrated as mentioned above (Fig. 2 and Fig. 4B), though notable sequence variation was observed between PtsN homologs of rhizobia and *E. coli* (Fig. 1B and C). Further protein interaction analysis revealed the GAF domain as the

minimum KdpD fragment interacting with $PtsN_1$ while the minimum region covering HisKA and HATPase domains interacting with KdpE (Fig. 6A and B). In *E. coli*, the region covering HisKA and HATPase domains interacts with KdpE, but PtsN interacts with HisKA (44, 46), i.e., apparently competing for binding (43). This paradox is largely resolved in *E. coli* by forming the PtsN/$KdpD_2$/KdpE ternary complex (46). Sequence analysis revealed that GAF of KdpD from SF4 and other rhizobia has additional N-terminal (from N496 to G529) and C-terminal (V650 to L672) fragments and more scattered polar residues (Q541, D570, T571, R588, R592, K601, T629, D641, and Q642) compared with GAF from *E. coli* (Fig. S2). Various GAF variants carrying substitutions at individual polar residues were constructed and tested for their interaction activity with $PtsN_1$ (Fig. 6C). It turned out that D517 located in the N-terminal fragment and D570, not present in GAF of *E. coli* KdpD, were the key residues involved in the interaction between GAF of KdpD and $PtsN_1$ in SF4. This novel interaction mechanism between KdpD and $EIIA^{Ntr}$ was further confirmed in the GST pulldown assay where intact GAF of KdpD rather than GAF(D517F) can effectively interact with $PtsN_1$ or $PtsN_2$ (Fig. 6D and E). Because the D517 carrying N-terminal fragment is also present in KdpD of many other rhizobia (Fig. S2), this signal transduction mechanism represents a novel model alternative to the well-known PtsN/$KdpD_2$/KdpE ternary binding model based on findings in *E. coli* (43, 46).

KdpE directly binds the promoter of *kdpFABC* but not those of *trkA* and *kup*. In addition to the high-affinity K^+ uptake system KdpFABC, the genome of SF4 harbors homologs of low-affinity TrkA and Kup systems (Fig. 7A) (24, 47, 48). qRT-PCR analysis of SF4 revealed that *kup* was downregulated while *kdp* was strongly upregulated under the low K^+ condition compared to the replete K^+ condition (Fig. 7B). By contrast, the *trkA* gene was transcribed at a relatively lower level compared with the other two systems when replete K^+ was supplied in the minimum medium, and it was slightly upregulated in the low K^+ medium (Fig. 7B). Further electrophoretic mobility shift assay (EMSA) showed that KdpE can directly binds the promoter region of *kdpFABC* operon but not those of *trkA* and *kup* (Fig. 7C). Therefore, the direct activation of *kdpFABC* operon by KdpE (43) also function in *S. fredii*.

The role of $EIIA^{Ntr}$-KdpDE-KdpFABC pathway during early symbiotic interactions. The above-mentioned direct evidences support a $EIIA^{Ntr}$-KdpDE-KdpFABC pathway in *S. fredii*, mediated by a non-canonical $EIIA^{Ntr}$-KdpD-KdpE binding model. It is noteworthy that SF4 derivatives carrying the phosphorylated form of $PtsN_1$(H66E) or lacking *kdpBC* formed less nodules on soybean plants while the number of nodules induced by the *kdpDE* mutant was not significantly different from that of the wild-type SF4 (Fig. 4A and D). Transcriptional profiles of *kdp*, *trkA*, and *kup* genes were determined under both low and replete K^+ conditions (Fig. S3). The deletion of *kdpDE* led to low transcription of the high-affinity KdpFABC system compared with SF4 as expected (Fig. S3), whereas the *kup* gene was strongly upregulated under the low K^+ condition (Fig. S3A; around 50-fold increase compared with SF4) though downregulated when 10 mM K^+ was supplied (Fig. S3B). For those strains forming less nodules such as the *$ptsN_1$(H66E)* and *kdpBC* strains, the *kup* and/or *trkA* were downregulated under the low K^+ condition (Fig. S3). By contrast, the *$ptsN_1$(H66A)* strain forming more nodules had a significant higher transcriptional level of *kdp* under both low and replete K^+ conditions, though *trkA* and *kup* were downregulated under the low K^+ condition (Fig. S3). The cumulative contribution of different K^+ uptake systems to nodulation was also observed in the *S. meliloti*-alfalfa symbiosis (24). In this work, we further revealed that the optimal nodulation in the *S. fredii*-soybean system is modulated by the $EIIA^{Ntr}$-KdpDE-KdpFABC pathway. Further exploring host responses to the *kdpBC* mutant during early symbiotic interaction stages (2-h, 4-h, 6-h, 8-h, 24-h, 2-days, and 4-days postinoculation) revealed an impaired transcription of the indispensable nodule inception regulator gene *NIN* and nodule primordium initiation marker gene *ENOD40* (28, 49–51) in soybean roots (Fig. 8A). This is consistent with the significantly delayed nodulation of the *kdpBC* mutant compared with the wild-type SF4 (Fig. 8B). Taken together with the findings on rhizoplane colonization and nodule occupancy, it seems that rhizobial K^+ uptake modulated by the PTS^{Ntr}-KdpDE-KdpFABC is crucial during early symbiotic interactions (Fig. 8C).

Conclusion. Despite the expansion of PtsN homologs in *S. fredii*, $PtsN_1$ is the major $EIIA^{Ntr}$ functioning in low K^+ adaptation and optimal nodulation, which are mediated by the two-component system KdpDE and the high-affinity K^+ uptake system KdpFABC. The sensor

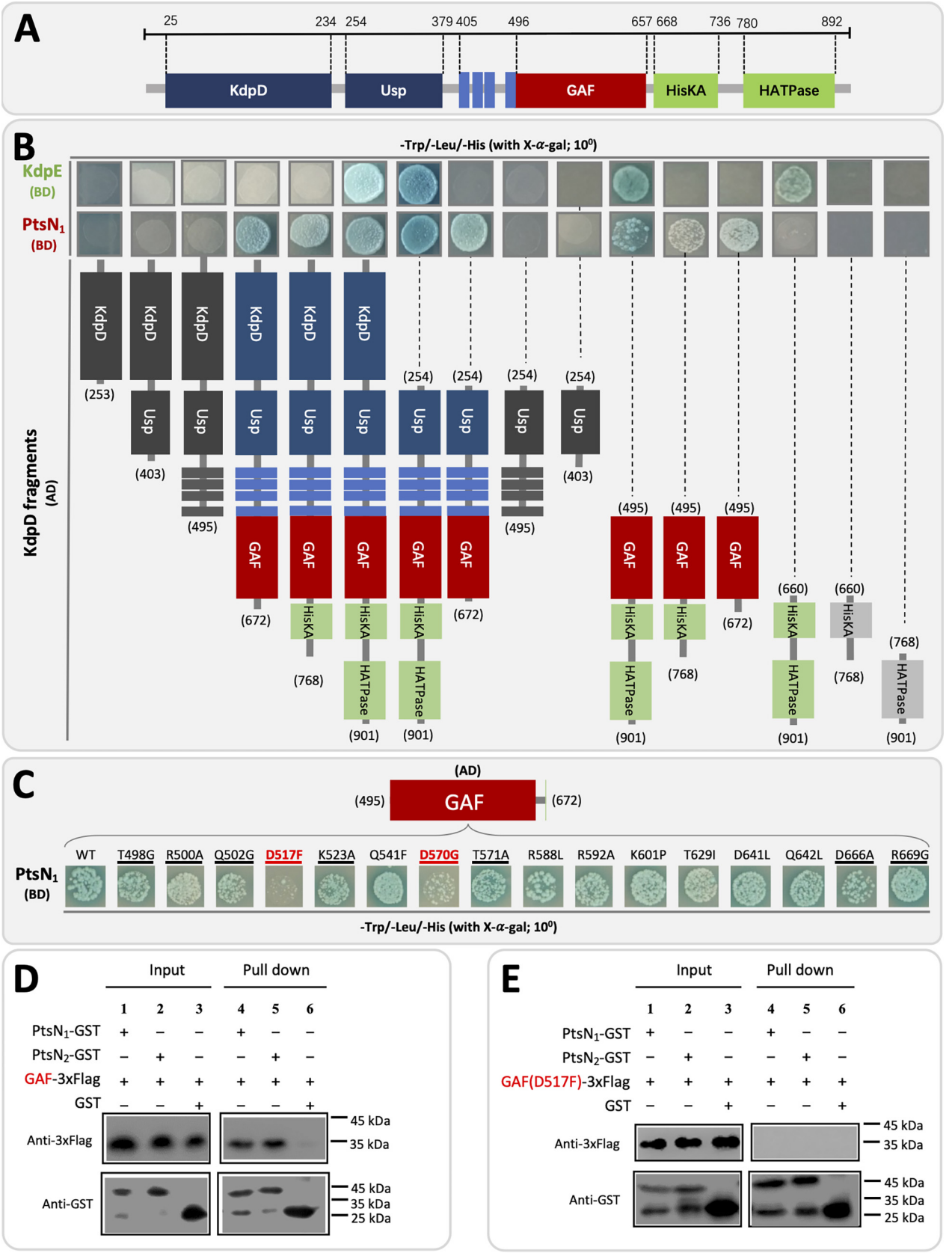

FIG 6 KdpD interacts with KdpE and $PtsN_1$ by HisKA-HATPase and GAF, respectively. (A) Schematic view of KdpD domains. Four transmembrane domains are indicated in light blue. (B) Identification of KdpD fragments (AD) interacting with KdpE (BD) and $PtsN_1$ (BD), respectively by using the

(Continued on next page)

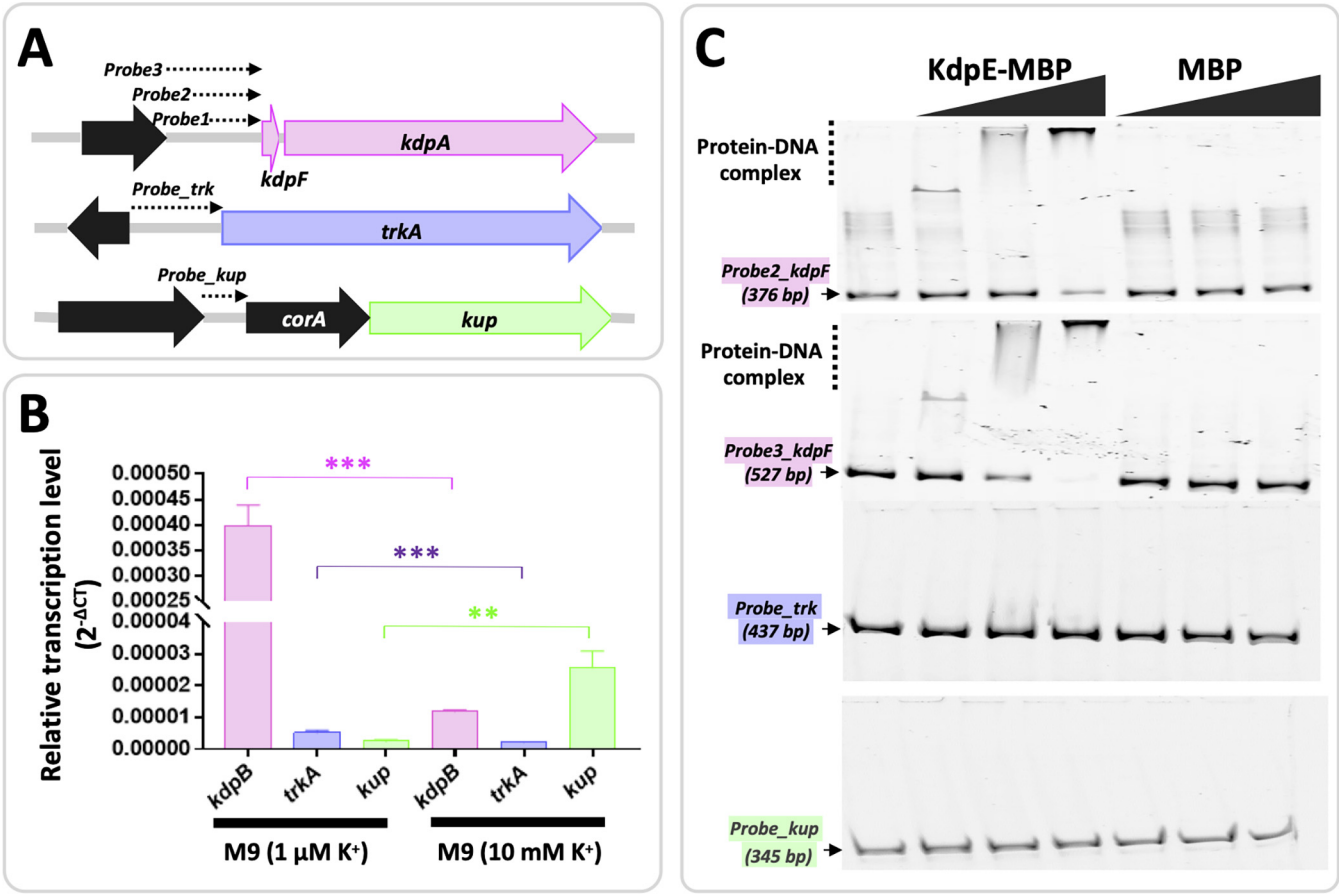

FIG 7 KdpE binds promoter of *kdpFABC* but not those of *trkA* and *kup*. (A) Promoters of *kdpFABC*, *trkA* and *kup*. The positions of probes used in electrophoretic mobility shift assay (EMSA) are indicated. *corA* encodes a putative transport protein for magnesium and cobalt. (B) qRT-PCR analysis of *kdpB*, *trkA*, and *kup* genes in SF4 under 1 μM and 10 mM K^+ conditions in the M9 minimum medium. 16S rRNA gene is used as the reference gene. (C) EMSA of KdpE with *kdpFABC*/*trkA*/*kup* promoter regions. The purified KdpE-MBP and MBP (5/20/50 μM) were incubated with Cy5-labeled DNA probes (12.3 nM). KdpE-MBP did not bind the *Probe1_kdpF* and the result is not shown herein.

kinase KdpD interacts with the unphosphorylated form of $EIIA^{Ntr}$ in a novel mechanism via its GAF domain, and with the response regulator KdpE via the HisKA-HATPase fragment. KdpE directly activates the transcription of the *kdpFABC* operon. Disruption of this pathway leads to defects in low K^+ adaptation and competitive nodulation. The *kdpBC* mutant has a reduced nodulation ability compared with WT while showing no severe impairment in rhizoplane colonization. This can be at least partially explained by the impaired induction of host nodulation genes by the *kdpBC* mutant and its delayed nodulation. Collectively, these findings suggest that K^+ uptake regulated by the PTS^{Ntr}-KdpDE-KdpFABC pathway is involved in optimizing early symbiotic interactions, highlighting a largely unexplored regulation of symbiosis by fluctuating nutrients in soils (31). K^+ is needed by all cellular organisms (43) and its role as an environmental cue in bacteria-host interactions is just emerging (26).

MATERIALS AND METHODS

Strains, plasmids, primers, and growth conditions. Strains and plasmids used in this study are listed in Table S5. All primers are shown in Table S6. *S. fredii* strains were grown at 28°C in Tryptone-Yeast (TY) (52) or modified-M9 minimal medium (53), with 1 μM, 1 mM, 5 mM, 10 mM, or 20 mM KCl supplied as indicated. *E. coli* was grown at 37°C in Luria-Bertani (LB) medium. *Saccharomyces cerevisiae* was grown at 30°C in

FIG 6 Legend (Continued)
yeast two-hybrid experiment. (C) Exploring screen of polar residues in the GAF domain involved in interacting with $PtsN_1$. Amino acid substitutions are indicated and residues located in either N-terminal or C-terminal fragments which are present in various rhizobia but absent in *E. coli* are underlined. In the yeast two-hybrid experiment (B to C), pGADT7/pGBKT7 and pGADT7-T/pGBKT7-53 were used as negative and positive controls, respectively, as shown in Fig. 2. The relative position of domains and residues within KdpD are shown when necessary. (D) Interaction between $PtsN_1$ or $PtsN_2$ with the GAF domain of KdpD by using GST pulldown assay. (E) GAF(D517F) unable to interact with $PtsN_1$ or $PtsN_2$ in the GST pulldown assay.

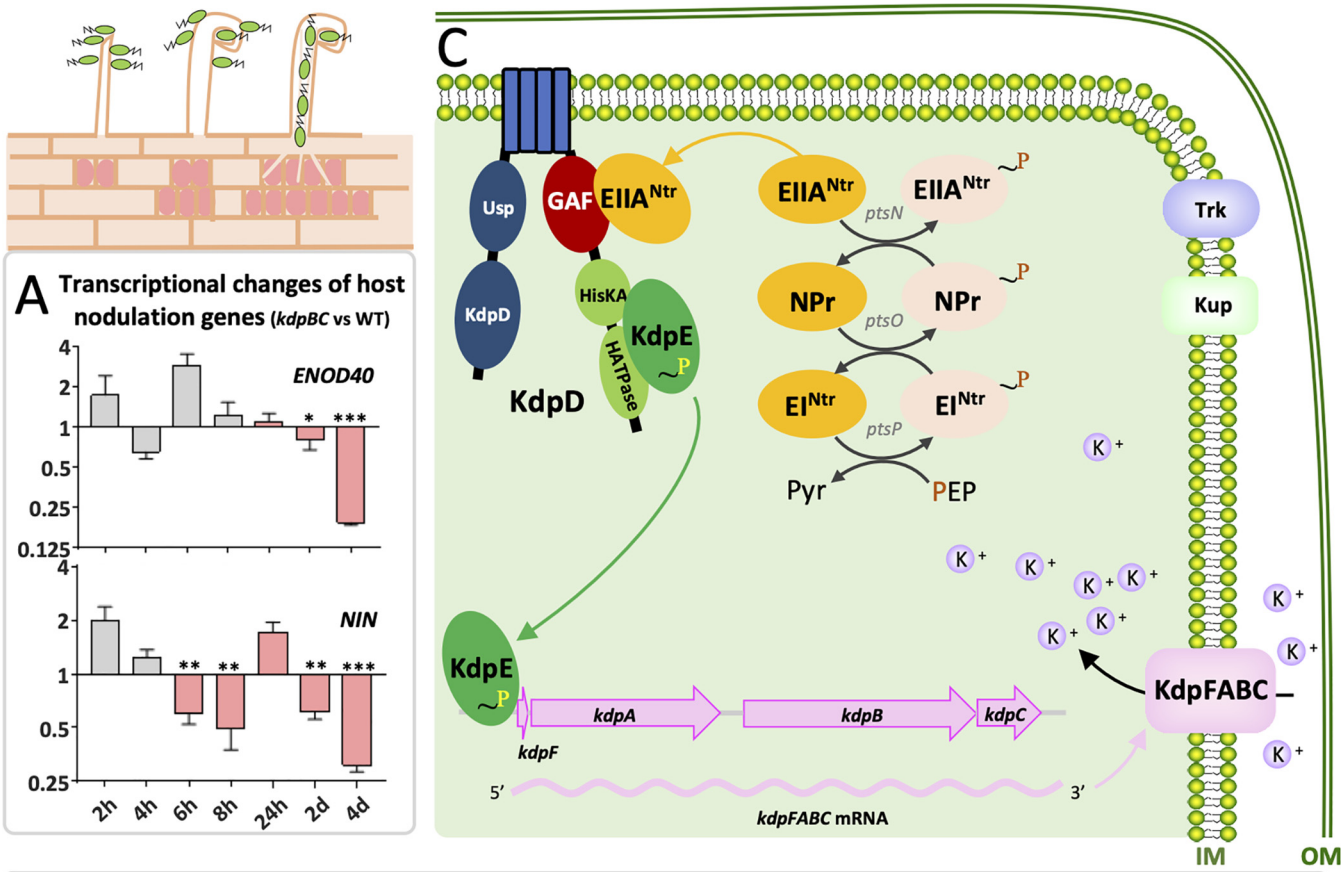

FIG 8 Regulation of K^+ uptake by the PTS^{Ntr}-KdpDE-KdpFABC pathway in nodulation. (A) Down regulation of *NIN* and *ENOD40* in roots inoculated with the *kdpBC* mutant compared with those in roots treated with the wild-type SF4. Hours (h) or days (d) postinoculation are shown corresponding to the early symbiotic interaction stages. The red bars represent a significant upregulation in the WT treatment compared with the uninoculated roots. Significant differences in gene transcriptional levels between the *kdpBC* treatment and the WT treatment are indicated (Student's *t* test; *, $P < 0.05$; **, $P < 0.01$; ***, $P < 0.001$). Error bars represent SE of the mean of three biological replicates. (B) Delayed nodulation of the *kdpBC* mutant compared with SF4 (dpi, days postinoculation). Significant differences in nodule number between two treatments are indicated (Student's *t* test; **, $P < 0.01$; ****, $P < 0.0001$). Error bars represent SE (based on data from two independent experiments; 6 to 11 plants were scored at each time point in each independent experiment). White triangles indicate position of nodules. Scale bars, 1 cm. (C) During nodulation, unphosphorylated form of $EIIA^{Ntr}$ interacts with the GAF domain of KdpD, which activates KdpE through the direct interaction between KdpE and the HisKA-HATPase region of KdpD. The active KdpE in turn binds the promoter of the *kdpFABC* operon to upregulate the transcription of this high-affinity K^+ uptake system.

Yeast-Peptone-Dextrose (YPD) medium (yeast extract 10 g/L, peptone 20 g/ L, glucose 20 g/ L). Antibiotics were added when necessary as described previously (29, 31). The Bioscreen C (Oy Growth Curves Ab Ltd, Raisio, Finland) was used to determine growth curves of test strains.

Plant assays, competitive nodulation, and rhizoplane colonization. Seeds of soybean cultivar JD17 (54) were treated with 95% ethanol for 30 s, then surface sterilized in 17% (vol/vol) NaClO for 3 min, and washed five to seven times using autoclaved deionized water. These seeds were germinated on 0.5% agar plates at 28°C in the dark for 48 h. Seedlings were inoculated with 1 mL of rhizobial suspension with OD_{600} = 0.2 in 0.8% (wt/vol) NaCl solution, and cultivated in vermiculite moistened with low-N nutrient solution [$Ca(NO_3)_2{\cdot}4H_2O$ 0.03 g, KCl 0.075 g, $MgSO_4$ 0.06 g, K_2HPO_4 0.136 g, $CaSO_4{\cdot}2H_2O$ 0.46 g, $FeC_6H_5O_7$ 0.075 g, H_3BO_3 2.86 mg, $MnSO_4$ 1.81 mg, $CuSO_4{\cdot}5H_2O$ 0.8 mg, $ZnSO_4$ 0.22 mg, H_2MoO_4 0.02 mg in one L medium]. When necessary, 10 mM KCl

was added into the low-N nutrient solution. Plants were harvested 30 days postinoculation or as indicated for nodule kinetics assay. The leaf chlorophyll content and shoot dry weight were determined as described previously (29). To determine nodule occupancy of rhizobia, the mutants were mixed with their parent strains at 1:1 (OD_{600} = 0.2) and inoculated on soybean plants. At 30 dpi, nodules were surface sterilized and nodulating strains were identified by their growth on TY plates with or without corresponding antibiotics as described previously (29). The identity of strains was further verified by PCR using primers targeting strain-specific fragments. The rhizoplane colonization ability was determined using the procedure described previously (31). Briefly, five to six germinated seeds were transferred to sterile petri dishes (diameter, 9 cm) which have low-N nutrient medium with 0.8% agar and filter paper. The mutants were mixed with their parent strains in equal quantity and inoculated (OD_{600}=0.2) on seedlings. At 7 dpi, roots were washed with water for three times and suspended in 0.85% NaCl solution. After exposure to six cycles of 30-s ultrasound treatment, the suspension was diluted and plated on TY plates with corresponding antibiotics. Colonies were counted and used for PCR verification of bacterial identity.

In-frame deletion and point mutation in *S. fredii*. In-frame deletion of *ptsN* homologs and *kdp* genes were performed using the seamless assembly cloning kit (Taihe Biotechnology, Beijing, China) with various pJQ200SK (55) derivatives carrying corresponding upstream and downstream homologous fragments using the procedure described previously (36). Upstream and downstream fragments were obtained by PCR using primers carrying sequences corresponding to the ends of SpeI restriction sites in pJQ200SK. The resultant homologous fragments were mixed with the linearized pJQ200SK (digested by SepI) in the reaction buffer that was further incubated at 50°C for 15 min before the transformation experiment with *E. coli* DH5α. The correct engineered plasmids harbored by positive clones were verified using PCR and Sanger sequencing, and then conjugated into *S. fredii* strains with the helper plasmid pRK2013 (56). Single-crossover clones resistant to gentamicin were further subject to counterselection for double recombinants using 5% sucrose. Double-crossover clones were verified by colony PCR and Sanger sequencing.

The *$ptsN_1$(H66A)*, *$ptsN_1$(H66E)*, and *$ptsN_1$.c* strains were constructed using the seamless assembly cloning kit (Taihe Biotechnology, Beijing, China) with pVO155 (57) derivatives carrying the wild-type *$ptsN_1$* sequence (*ptsN1.c*) or its mutated forms (H66A: CAC to TGC; H66E: CAC to TTC). The pVO155 was linearized by BamHI and XbaI, and mixed with the corresponding *$ptsN_1$* fragments in the reaction buffer, and incubated at 50°C for 15 min. The resultant plasmids were transformed into *E. coli* DH5α and positive clones were verified by PCR and Sanger sequencing. The plasmids were then conjugated into the *$ptsN_1$* mutant with the helper plasmid pRK2013 and single-crossover clones resistant to kanamycin were verified by colony PCR and Sanger sequencing.

Yeast two-hybrid assay. By using the seamless assembly cloning method as described above, $PtsN_1$, $PtsN_2$, $PtsN_3$, KdpE, KdpD, different fragments of KdpD, or mutated GAF of KdpD were fused to either the GAL4 activation domain (AD; pGADT7) or DNA-binding domain (BD; pGBKT7) to generate various derivatives which were then transformed into *E. coli* DH5α and positive clones were verified by PCR and Sanger sequencing. The extracted various AD and BD plasmids were cointroduced into *Saccharomyces cerevisiae* AH109. The yeast two-hybrid assay was performed according to the manual of Matchmaker GAL4 two-hybrid system 3 (TaKaRa Bio).

Protein purification, pulldown assay, and Western blot analysis. Sequences corresponding to GAF of KdpD, GAF(D517F), $PtsN_1$, $PtsN_2$, and KdpE were amplified using related primers as shown in Table S6. The resultant fragments were ligated into expression vector pET-28a(+), pGEX-4T-1, or pMAL-c5x, and transformed into *E. coli* BL21(DE3), generating the GAF-3×Flag, GAF(D517F)-3×Flag, $PtsN_1$-GST, $PtsN_2$-GST, and KdpE-MBP expression vectors. Cultures of OD_{600} = 0.4 to 0.6 were subject to induction with 0.1 mM IPTG (Coolaber) for 14 h at 16°C. Cells were then harvested, washed, and resuspended using lysis buffer with protease inhibitor cocktail (Coolaber), and sonicated on ice. GAF-3×Flag and GAF (D517F)-3×Flag cell extracts were loaded onto Nickel-IDA agarose beads (GenStar), and KdpE-MBP cell extracts were loaded onto Amylose Resin (BioLabs) for protein purification.

To perform GST pulldown assay, $PtsN_1$-GST and $PtsN_2$-GST cell extracts were incubated with GST beads for 3 h at 4°C, and washed three times with low salt buffer (20 mM Tris-HCl [pH 7.5], 150 mM NaCl, 0.1% Triton X-100, and protease inhibitor cocktail [Coolaber]). Then the beads were incubated in blocking buffer (20 mM Tris-HCl [pH 7.5], 150 mM NaCl, 0.1% Triton X-100, 5% BSA, protease inhibitor cocktail) for 1h at 4°C. The beads were incubated with GAF-3×Flag or GAF(D517F)-3×Flag proteins at 4°C for 1h. Finally, the beads were collected and washed three to five times with low salt buffer and high salt buffer (20 mM Tris-HCl [pH 7.5], 300 mM NaCl, 0.1% Triton X-100, protease inhibitor cocktail). The proteins eluted from beads were then used for Western bolt analysis.

Proteins were added into 5× loading buffer, then boiled 5 min, and electrophoresed on 10% SDS-PAGE gels. Monoclonal mouse antibody against 3×Flag epitope (Sigma) or GST (Sigma) epitope and the horseradish peroxidase (HPR)-conjugated goat anti-mouse immunoglobulin G (IgG) secondary antibody (ZSGB-BIO) were used at 1:500 and 1:1,000 dilution ratios. Signals of the protein on X-ray film were recorded by chemiluminescence detection.

Electrophoretic mobility shift assay. The Cy5-DNA probes (*Probe1_kdpF*, *Probe2_kdpF*, *Probe3_kdpF*, *Probe_trk*, and *Probe_kup*) within the putative promoter regions of *kdpFABC*, *trkA*, or *kup* were amplified with related primers labeled with Cy5 at 5′ ends (Table S6). Different quantity of purified KdpE-MBP or MBP (5, 20, 50 μM) and 12.3 nM individual Cy5-DNA probes were added into the 10 μL reaction mixture (0.5 mg/mL BSA, 0.1 mg/mL sonicated salmon sperm DNA, 25 mM Tris-HCl [pH 8.0], 5% glycerol, 0.05% DDM) and incubated at 20°C for 30 min. The resultant samples were separated in a 6% (wt/vol) native polyacrylamide gel and visualized with a Typhoon FLA 9000 imager (GE Healthcare).

The *kdpFABC* operon determination and quantitative real-time PCR. To determine the cotranscription of *kdpF*, *kdpA*, *kdpB*, and *kdpC*, reverse transcription-PCR was conducted. The concentration of mid-log-phase cultures was adjusted to OD_{600} = 0.2 and cultured in modified M9 minimal medium for 9 h. RNA was extracted using a Bacteria Total RNA Kit (Zomanbio). cDNA was synthesized using Reverse

Transcriptase Kit (Zomanbio). Primers targeting for intergenic regions of *kdpF-kdpA*, *kdpA-kdpB*, or *kdpB-kdpC* were used to test the cotranscription profiles in cDNA, with DNA as control samples.

To determine the transcriptional profiles of *kdpB*, *trkA*, and *kup* in various test strains, rhizobia were cultivated in modified M9 minimum medium (supplied with 1 μM or 10 mM KCl) for 9 h as described above. Extraction of rhizobial RNA and cDNA synthesis were carried out using the same method described above. To test the transcriptional levels of *NIN* and *ENOD40* in soybean roots during early symbiotic interactions, roots from soybean plants inoculated with the *kdpBC* mutant or the wild-type SF4 were collected at 2-h, 4-h, 6-h, 8-h, 24-h, 2-days and 4-days postinoculation, and the uninoculated roots at the same stages were used as control. The Total RNA Extraction Kit (Promega) and Reverse Transcriptase Kit (Genestar) were used to obtain root RNA and cDNA. The qRT-PCR was performed with corresponding gene-specific primers using RealStar Green Fast Mixture (Genestar) and an ABI QuantStudioT^6 Flex System real-time PCR system. Transcription levels were normalized to the expression of the internal control gene 16s rRNA (bacteria) or 18s rRNA (plants). Three biological replicates were performed.

Phylogenetic analysis. Protein sequences of PtsN homologs were extracted from the GenBank database, aligned with ClustalW, and used in the maximum likelihood phylogenetic tree reconstruction by MEGA5 (58) with default parameters. The tree was tested by 1,000 bootstrap replicates.

SUPPLEMENTAL MATERIAL

Supplemental material is available online only.

FIG S1, PDF file, 0.2 MB.

FIG S2, PDF file, 0.5 MB.

FIG S3, PDF file, 0.2 MB.

TABLE S1, PDF file, 0.1 MB.

TABLE S2, PDF file, 0.1 MB.

TABLE S3, PDF file, 0.1 MB.

TABLE S4, PDF file, 0.1 MB.

TABLE S5, XLSX file, 0.02 MB.

TABLE S6, XLSX file, 0.02 MB.

ACKNOWLEDGMENTS

We thank Huiqiang Lou and Jie Hao from Prof. Weihua Wu's group for providing vectors used in the yeast two-hybrid assay and the pMAL-c5x vector, respectively. This work was supported by the National Key R&D Program of China (grant number 2019YFA0904700), National Natural Science Foundation of China (grant number 32070078), the Innovative Project of State Key Laboratory of Agrobiotechnology (grant number 2020SKLAB1-5), and the 2115 Talent Development Program of China Agricultural University.

C.F.T., W.X.C., and X.Y.F. planned and designed the research; X.Y.F., Y.T., W.J.C., Y.Z.L., D.W., Y.L., and J.J. performed experiments and analyzed data; C.F.T. and X.Y.F. wrote the manuscript.

We declare that they have no competing interests.

REFERENCES

1. Mijakovic I, Macek B. 2012. Impact of phosphoproteomics on studies of bacterial physiology. FEMS Microbiol Rev 36:877–892. https://doi.org/10.1111/j.1574-6976.2011.00314.x.
2. Hanks SK, Quinn AM, Hunter T. 1988. The protein kinase family: conserved features and deduced phylogeny of the catalytic domains. Science 241:42–52. https://doi.org/10.1126/science.3291115.
3. Grangeasse C, Cozzone AJ, Deutscher J, Mijakovic I. 2007. Tyrosine phosphorylation: an emerging regulatory device of bacterial physiology. Trends Biochem Sci 32:86–94. https://doi.org/10.1016/j.tibs.2006.12.004.
4. Buschiazzo A, Trajtenberg F. 2019. Two-component sensing and regulation: how do histidine kinases talk with response regulators at the molecular level? Annu Rev Microbiol 73:507–528. https://doi.org/10.1146/annurev-micro-091018-054627.
5. Pflüger-Grau K, Görke B. 2010. Regulatory roles of the bacterial nitrogen-related phosphotransferase system. Trends Microbiol 18:205–214. https://doi.org/10.1016/j.tim.2010.02.003.
6. Deutscher J, Aké FMD, Derkaoui M, Zébré AC, Cao TN, Bouraoui H, Kentache T, Mokhtari A, Milohanic E, Joyet P. 2014. The bacterial phosphoenolpyruvate:carbohydrate phosphotransferase system: Regulation by protein phosphorylation and phosphorylation-dependent protein-protein interactions. Microbiol Mol Biol Rev 78:231–256. https://doi.org/10.1128/MMBR.00001-14.
7. Lengeler JW. 2015. PTS 50: past, present and future, or diauxie revisited. J Mol Microbiol Biotechnol 25:79–93. https://doi.org/10.1159/000369809.
8. Lüttmann D, Göpel Y, Görke B. 2012. The phosphotransferase protein EIIA(Ntr) modulates the phosphate starvation response through interaction with histidine kinase PhoR in *Escherichia coli*. Mol Microbiol 86:96–110. https://doi.org/10.1111/j.1365-2958.2012.08176.x.
9. Sánchez-Cañizares C, Prell J, Pini F, Rutten P, Kraxner K, Wynands B, Karunakaran R, Poole PS. 2020. Global control of bacterial nitrogen and carbon metabolism by a PTS^{Ntr}-regulated switch. Proc Natl Acad Sci U S A 117:10234–10245. https://doi.org/10.1073/pnas.1917471117.
10. Korolev N. 2021. How potassium came to be the dominant biological cation: of metabolism, chemiosmosis, and cation selectivity since the beginnings of life. BioEssays 43:2000108–2000118. https://doi.org/10.1002/bies.202000108.
11. Corratgé-Faillie C, Jabnoune M, Zimmermann S, Véry A-A, Fizames C, Sentenac H. 2010. Potassium and sodium transport in non-animal cells: the Trk/Ktr/HKT transporter family. Cell Mol Life Sci 67:2511–2532. https://doi.org/10.1007/s00018-010-0317-7.
12. Diskowski M, Mikusevic V, Stock C, Hänelt I. 2015. Functional diversity of the superfamily of K^+ transporters to meet various requirements. Biol Chem 396:1003–1014. https://doi.org/10.1515/hsz-2015-0123.

13. Huang C, Pedersen BP, Stokes DL. 2017. Crystal structure of the potassium-importing KdpFABC membrane complex. Nature 546:681–685. https://doi.org/10.1038/nature22970.
14. Pedersen BP, Stokes DL, Apell HJ. 2019. The KdpFABC complex–K^+ transport against all odds. Mol Membr Biol 35:21–38. https://doi.org/10.1080/09687688.2019.1638977.
15. Lüttmann D, Heermann R, Zimmer B, Hillmann A, Rampp IS, Jung K, Görke B. 2009. Stimulation of the potassium sensor KdpD kinase activity by interaction with the phosphotransferase protein IIA^{Ntr} in *Escherichia coli*. Mol Microbiol 72:978–994. https://doi.org/10.1111/j.1365-2958.2009.06704.x.
16. Prell J, Mulley G, Haufe F, White JP, Williams A, Karunakaran R, Downie JA, Poole PS. 2012. The PTS^{Ntr} system globally regulates ATP-dependent transporters in *Rhizobium leguminosarum*. Mol Microbiol 84:117–129. https://doi.org/10.1111/j.1365-2958.2012.08014.x.
17. Deuschle M, Limbrunner S, Rother D, Wahler S, Chavarría M, de Lorenzo V, Kremling A, Pflüger-Grau K. 2015. Interplay of the PtsN ($EIIA^{Ntr}$) protein of *Pseudomonas putida* with its target sensor kinase KdpD. Environ Microbiol Rep 7:899–907. https://doi.org/10.1111/1758-2229.12323.
18. Liu Y, Ho KK, Su J, Gong H, Chang AC, Lu S. 2013. Potassium transport of *Salmonella* is important for type III secretion and pathogenesis. Microbiology (Reading) 159:1705–1719. https://doi.org/10.1099/mic.0.068700-0.
19. Gries CM, Bose JL, Nuxoll AS, Fey PD, Bayles KW. 2013. The Ktr potassium transport system in *Staphylococcus aureus* and its role in cell physiology, antimicrobial resistance and pathogenesis. Mol Microbiol 89:760–773. https://doi.org/10.1111/mmi.12312.
20. Stingl K, Brandt S, Uhlemann E-M, Schmid R, Altendorf K, Zeilinger C, Ecobichon C, Labigne A, Bakker EP, de Reuse H. 2007. Channel-mediated potassium uptake in *Helicobacter pylori* is essential for gastric colonization. EMBO J 26:232–241. https://doi.org/10.1038/sj.emboj.7601471.
21. MacGilvary NJ, Kevorkian YL, Tan S. 2019. Potassium response and homeostasis in *Mycobacterium tuberculosis* modulates environmental adaptation and is important for host colonization. PLoS Pathog 15:e1007591–23. https://doi.org/10.1371/journal.ppat.1007591.
22. Valente RS, Xavier KB. 2016. The Trk potassium transporter is required for RsmB-mediated activation of virulence in the phytopathogen *Pectobacterium wasabiae*. J Bacteriol 198:248–255. https://doi.org/10.1128/JB.00569-15.
23. Binepal G, Gill K, Crowley P, Cordova M, Brady LJ, Senadheera DB, Cvitkovitch DG. 2016. Trk2 potassium transport system in *Streptococcus mutans* and its role in potassium homeostasis, biofilm formation, and stress tolerance. J Bacteriol 198:1087–1100. https://doi.org/10.1128/JB.00813-15.
24. Dominguez-Ferreras A, Munoz S, Olivares J, Soto MJ, Sanjuan J. 2009. Role of potassium uptake systems in *Sinorhizobium meliloti* osmoadaptation and symbiotic performance. J Bacteriol 191:2133–2143. https://doi.org/10.1128/JB.01567-08.
25. Tan S. 2021. Abundant monovalent ions as environmental signposts for pathogens during host colonization. Infect Immun 89:e00641-20. https://doi.org/10.1128/IAI.00641-20.
26. Freeman ZN, Dorus S, Waterfield NR. 2013. The KdpD/KdpE two-component system: integrating K^+ homeostasis and virulence. PLoS Pathog 9:e1003201. https://doi.org/10.1371/journal.ppat.1003201.
27. Poole P, Ramachandran V, Terpolilli J. 2018. Rhizobia: from saprophytes to endosymbionts. Nat Rev Microbiol 16:291–303. https://doi.org/10.1038/nrmicro.2017.171.
28. Roy S, Liu W, Nandety RS, Crook A, Mysore KS, Pislariu CI, Frugoli J, Dickstein R, Udvardi MK. 2020. Celebrating 20 years of genetic discoveries in legume nodulation and symbiotic nitrogen fixation. Plant Cell 32:15–41. https://doi.org/10.1105/tpc.19.00279.
29. Li YZ, Wang D, Feng XY, Jiao J, Chen WX, Tian CF. 2016. Genetic analysis reveals the essential role of nitrogen phosphotransferase system components in *Sinorhizobium fredii* CCBAU 45436 symbioses with soybean and pigeonpea plants. Appl Environ Microbiol 82:1305–1315. https://doi.org/10.1128/AEM.03454-15.
30. Liu LX, Li QQ, Zhang YZ, Hu Y, Jiao J, Guo HJ, Zhang XX, Zhang B, Chen WX, Tian CF. 2017. The nitrate-reduction gene cluster components exert lineage-dependent contributions to optimization of *Sinorhizobium* symbiosis with soybeans. Environ Microbiol 19:4926–4938. https://doi.org/10.1111/1462-2920.13948.
31. Zhang P, Zhang B, Jiao J, Dai S-Q, Chen W-X, Tian C-F. 2020. Modulation of symbiotic compatibility by rhizobial zinc starvation machinery. mBio 11:e03193-19. https://doi.org/10.1128/mBio.03193-19.
32. Cui W-J, Zhang B, Zhao R, Liu L-X, Jiao J, Zhang Z, Tian C-F. 2021. Lineage-specific rewiring of core pathways predating innovation of legume nodules shapes symbiotic efficiency. mSystems 6:1–18. https://doi.org/10.1128/mSystems.01299-20.
33. Zimmer B, Hillmann A, Görke B. 2008. Requirements for the phosphorylation of the *Escherichia coli* $EIIA^{Ntr}$ protein *in vivo*. FEMS Microbiol Lett 286:96–102. https://doi.org/10.1111/j.1574-6968.2008.01262.x.
34. Sprent JI. 2007. Evolving ideas of legume evolution and diversity: a taxonomic perspective on the occurrence of nodulation. New Phytol 174:11–25. https://doi.org/10.1111/j.1469-8137.2007.02015.x.
35. Oono R, Schmitt I, Sprent JI, Denison RF. 2010. Multiple evolutionary origins of legume traits leading to extreme rhizobial differentiation. New Phytol 187:508–520. https://doi.org/10.1111/j.1469-8137.2010.03261.x.
36. Hu Y, Jiao J, Liu LX, Sun YW, Chen WF, Sui XH, Chen WX, Tian CF. 2018. Evidence for phosphate starvation of rhizobia without terminal differentiation in legume nodules. Mol Plant Microbe Interact 31:1060–1068. https://doi.org/10.1094/MPMI-02-18-0031-R.
37. Mergaert P, Uchiumi T, Alunni B, Evanno G, Cheron A, Catrice O, Mausset A-E, Barloy-Hubler F, Galibert F, Kondorosi A, Kondorosi E. 2006. Eukaryotic control on bacterial cell cycle and differentiation in the Rhizobium-legume symbiosis. Proc Natl Acad Sci U S A 103:5230–5235. https://doi.org/10.1073/pnas.0600912103.
38. Sun Y-W, Li Y, Hu Y, Chen W-X, Tian C-F. 2019. Coordinated regulation of the size and number of polyhydroxybutyrate granules by core and accessory phasins in the facultative microsymbiont *Sinorhizobium fredii* NGR234. Appl Environ Microbiol 85:e00717-19. https://doi.org/10.1128/AEM.00717-19.
39. Begon M, Townsend CR. 2021. Ecology: From individuals to ecosystems. Wiley, Hoboken, New Jersey.
40. Wang G, Peterkofsky A, Keifer PA, Li X. 2005. NMR characterization of the *Escherichia coli* nitrogen regulatory protein IIA^{Ntr} in solution and interaction with its partner protein, NPr. Protein Sci 14:1082–1090. https://doi.org/10.1110/ps.041232805.
41. Karstens K, Zschiedrich CP, Bowien B, Stülke J, Görke B. 2014. Phosphotransferase protein $EIIA^{Ntr}$ interacts with SpoT, a key enzyme of the stringent response, in *Ralstonia eutropha* H16. Microbiology (Reading) 160:711–722. https://doi.org/10.1099/mic.0.075226-0.
42. Lee C-R, Cho S-H, Yoon M-J, Peterkofsky A, Seok Y-J. 2007. *Escherichia coli* enzyme IIA^{Ntr} regulates the K^+ transporter TrkA. Proc Natl Acad Sci U S A 104:4124–4129. https://doi.org/10.1073/pnas.0609897104.
43. Danchin A, Nikel PI. 2019. Why nature chose potassium. J Mol Evol 87:271–288. https://doi.org/10.1007/s00239-019-09915-2.
44. Xie M, Wu M, Han A. 2020. Structural insights into the signal transduction mechanism of the K^+-sensing two-component system KdpDE. Sci Signal 13:1–12.
45. Lüttmann D, Göpel Y, Görke B. 2015. Cross-talk between the canonical and the nitrogen-related phosphotransferase systems modulates synthesis of the KdpFABC potassium transporter in *Escherichia coli*. J Mol Microbiol Biotechnol 25:168–177. https://doi.org/10.1159/000375497.
46. Mörk-Mörkenstein M, Heermann R, Göpel Y, Jung K, Görke B. 2017. Non-canonical activation of histidine kinase KdpD by phosphotransferase protein PtsN through interaction with the transmitter domain. Mol Microbiol 106:54–73. https://doi.org/10.1111/mmi.13751.
47. Dosch DC, Helmer GL, Sutton SH, Salvacion FF, Epstein W. 1991. Genetic analysis of potassium transport loci in *Escherichia coli*: Evidence for three constitutive systems mediating uptake of potassium. J Bacteriol 173:687–696. https://doi.org/10.1128/jb.173.2.687-696.1991.
48. Trchounian A, Kobayashi H. 1999. Kup is the major K^+ uptake system in *Escherichia coli* upon hyper-osmotic stress at a low pH. FEBS Lett 447:144–148. https://doi.org/10.1016/S0014-5793(99)00288-4.
49. Niwa S, Kawaguchi M, Imazumi-Anraku H, Chechetka SA, Ishizaka M, Ikuta A, Kouchi H. 2001. Responses of a model legume *Lotus japonicus* to lipochitin oligosaccharide nodulation factors purified from *Mesorhizobium loti* JRL501. Mol Plant Microbe Interact 14:848–856. https://doi.org/10.1094/MPMI.2001.14.7.848.
50. Wang Y, Wang L, Zou Y, Chen L, Cai Z, Zhang S, Zhao F, Tian Y, Jiang Q, Ferguson BJ, Gresshoff PM, Li X. 2014. Soybean miR172c targets the repressive AP2 transcription factor NNC1 to activate ENOD40 expression and regulate nodule initiation. Plant Cell 26:4782–4801. https://doi.org/10.1105/tpc.114.131607.
51. Griesmann M, Chang Y, Liu X, Song Y, Haberer G, Crook MB, Billault-Penneteau B, Lauressergues D, Keller J, Imanishi L, Roswanjaya YP, Kohlen W, Pujic P, Battenberg K, Alloisio N, Liang Y, Hilhorst H, Salgado MG, Hocher V, Gherbi H, Svistoonoff S, Doyle JJ, He S, Xu Y, Xu S, Qu J, Gao Q, Fang X, Fu Y, Normand P, Berry AM, Wall LG, Ané J-M, Pawlowski K, Xu X, Yang H, Spannagl M, Mayer KFX, Wong GK-S, Parniske M, Delaux P-M, Cheng S. 2018. Phylogenomics reveals multiple losses of nitrogen-fixing root nodule symbiosis. Science 361:eaat1743. https://doi.org/10.1126/science.aat1743.
52. Vincent JM. 1970. A manual for the practical study of root nodule bacteria. Blackwell, Oxford, United Kingdom.

53. Miller JH. 1972. Experiments in molecular genetics. Cold Spring Harbor Laboratory, Cold Spring Harbor, New York.
54. Qin J. 2014. A genetic composition analysis of soybean sibling varieties Jidou17 and Ji nf58. Aust J Crop Sci 8:791–798.
55. Quandt J, Hynes MF. 1993. Versatile suicide vectors which allow direct selection for gene replacement in Gram-negative bacteria. Gene 127:15–21. https://doi.org/10.1016/0378-1119(93)90611-6.
56. Ditta G, Stanfield S, Corbin D, Helinski DR. 1980. Broad host range DNA cloning system for Gram-negative bacteria: construction of a gene bank of Rhizobium meliloti. Proc Natl Acad Sci U S A 77:7347–7351. https://doi.org/10.1073/pnas.77.12.7347.
57. Oke V, Long SR. 1999. Bacterial genes induced within the nodule during the Rhizobium-legume symbiosis. Mol Microbiol 32:837–849. https://doi.org/10.1046/j.1365-2958.1999.01402.x.
58. Tamura K, Peterson D, Peterson N, Stecher G, Nei M, Kumar S. 2011. MEGA5: molecular evolutionary genetics analysis using maximum likelihood, evolutionary distance, and maximum parsimony methods. Mol Biol Evol 28:2731–2739. https://doi.org/10.1093/molbev/msr121.